https://doi.org/10.5194/egusphere-2026-4374
Preprint. Discussion started: 29 July 2026

ICE-NADI-1: A new deglacial ice sheet thickness history (25-1 ka) for North America using empirically-constrained ice margins with implications for global sea-level contributions, relative sea level, and vertical land motion

Erica M. Lucas[1], Samuel Kodama[1], Tamara Pico[1], Benjamin J. Stoker[2], Alia J. Lesnek[3,4], April S. Dalton[5]

[1] Earth & Planetary Sciences, University of California, Santa Cruz
[2] Lamont Doherty Earth Observatory, Columbia University
[3] School of Earth and Environmental Sciences, CUNY Queens College
[4] Earth and Environmental Sciences, CUNY Graduate Center
[5] Centre Geotop, Université du Québec à Montréal, Montréal, QC, Canada

Correspondence to: Erica M. Lucas (ermlucas@ucsc.edu)

Abstract. We generate three new empirically-based deglacial ice sheet histories (ice sheet thickness reconstructions) of the North American Ice Sheet Complex (ICE-NADI-1, ICE-NADI-1_min, and ICE-NADI-1_max) from 25 ka to 1 ka in 500-year intervals using a simple, steady-state numerical ice sheet model. To build the ice sheet histories, we adopt the North America Deglaciation Isochrones (NADI-1; Dalton et al., 2023). Our new ICE-NADI-1 ice sheet thickness reconstruction contains a peak North American sea-level equivalent (SLE) ice volume of 64 m of at the Last Glacial Maximum, 25% smaller than the North American ice volume contained within ICE-7G (Roy & Peltier, 2017). North American ice saddle merging contributes 13 m SLE to global sea-level fall leading into the Last Glacial Maximum. Across Meltwater Pulse 1a (14.5-14 ka), our ICE-NADI-1 ice sheet thickness reconstruction contributes 6.3 m SLE, and the peak ice loss rate (13 mm SLE/year) is less than half the rate of ice loss in ICE-7G.

Glacial isostatic adjustment simulations show that our new ICE-NADI-1 ice sheet thickness reconstruction fits relative sea-level observations across North America as well or better than previous reconstructions. Predicted present-day vertical land motion with ICE-NADI-1 differs from previous predictions by up to 9 mm per year. Because NADI-1 ice margins capture geologic uncertainty in ice margin, we are able to quantitatively assess the sensitivity of glacial isostatic adjustment predictions (relative sea level, paleotopography, and present-day vertical land motion) to ice geometry, which previously has not been possible. We find this uncertainty comparable in magnitude to that associated with unknowns in Earth structure. Ultimately, our ice sheet thickness reconstructions illustrate how 2-D ice margins inform the history of ice volume evolution, granting new insight into North American Ice Sheet Complex dynamics and the associated changes in global sea level, relative sea level, and vertical land motion.

1 Introduction

The North American Ice Sheet Complex, comprised of the Laurentide, Cordilleran, and Innuitian ice sheets, was the largest continental ice sheet in the Northern Hemisphere during the Last Glacial Maximum (LGM; ~26-19 ka; Clark et al., 2009). Yet the history of North American ice sheet thickness over the last deglaciation remains poorly constrained (Stokes et al., 2015). Existing glacial isostatic adjustment (GIA) predictions for previously-glaciated sectors of North America misfit relative sea-level and geodetic observations across a range of timescales (deglacial to modern; Engelhart & Horton, 2012; Peltier et al., 2014; Engelhart et al., 2015; Yousefi et al., 2018; Vacchi et al., 2018). These misfits highlight major unknowns in both the ice loading history and Earth structure, the two key inputs to GIA modeling, underscoring the need to build accurate ice sheet thickness reconstructions to improve GIA predictions and our inferences of Earth structure.

To date, a number of efforts have reconstructed the thickness of the North American Ice Sheet Complex, including approaches that (1) fit far-field sea-level records and modern geodetic observations but do not capture realistic ice physics (ICE-XG; e.g., Peltier, 2004; Peltier et al., 2015; Roy & Peltier, 2017), (2) adjust glaciologically-constrained models using regional ice thickness scaling parameters (LW-6; Lambeck et al., 2017), (3) adopt numerical ice sheet models with simplified ice physics (NAICE; Gowan et al., 2016b), and (4) average thousands of numerical ice sheet simulations (e.g., GLAC-1D; Tarasov et al., 2012). Most of these numerical studies hinged their work on the ice margin reconstructions of Dyke et al. (2003) and Dyke (2004) (which will hereafter be referred to as the Dyke (2004) margins).

A new set of North American ice margins, the North American Deglaciation Isochrones (NADI-1; Dalton et al., 2023) incorporate updated chronological constraints combined with geomorphological evidence to reconstruct deglacial ice margins at 500-year timesteps (Fig. 1). Furthermore, the NADI-1 margins include optimal, minimum, and maximum margins designed to capture uncertainty related to dating method or conflicting chronological constraints. Not only do the NADI-1 margins capture the retreat of the North American ice sheet, but they also capture ice sheet advances, especially between 25 and 20 ka, although this interval is characterized by greater uncertainty due to sparse geochronological data from this period (Dalton et al., 2023). For example, NADI-1 optimal margins capture the asynchronous nature of the Last Glacial Maximum across North America: with some sectors of the ice sheet complex reaching maximum extent at 25 ka and others later at 18.5-17.5 ka. According to the NADI-1 optimal margins, the Cordilleran and Laurentide ice sheets merged at 22.5 ka and the subsequent saddle collapse occurred at 14 ka. To date, the NADI-1 ice margins have not been leveraged as constraints on ice volume and global sea-level change.

Here we present North American Ice Sheet Complex thickness reconstructions (ICE-NADI-1, ICE-NADI-1_min, ICE-NADI-1_max) over the last deglaciation (25 ka to 1 ka) at 0.5 ky time intervals using the NADI-1 optimal, minimum, and maximum margins. Our work uses the NADI-1 ice margins (Dalton et al., 2023) in a numerical, steady-state, ice sheet model with simple

https://doi.org/10.5194/egusphere-2026-4374
Preprint. Discussion started: 29 July 2026

ice physics (ICESHEET; Gowan et al., 2016a) to reconstruct North American Ice Sheet Complex ice thickness. The uncertainty bounds on NADI-1 ice margins permit a quantitative assessment of the sensitivity of relative sea-level predictions to ice geometry, which has not been possible previously. We explore how uncertainty associated with the NADI-1 margins impacts our understanding of ice sheet volume evolution over the deglaciation. Our three new North American ice thickness reconstructions (ICE-NADI-1, ICE-NADI-1_min, ICE-NADI-1_max) are patched into the global ice sheet history ICE-6G_C (Peltier et al., 2015) and are publicly available for use in GIA simulations and other analyses (https://doi.org/10.5281/zenodo.21464139; Lucas et al., 2026). We show that our new ice sheet thickness reconstructions fit relative sea-level observations across North America as well or better than existing reconstructions.

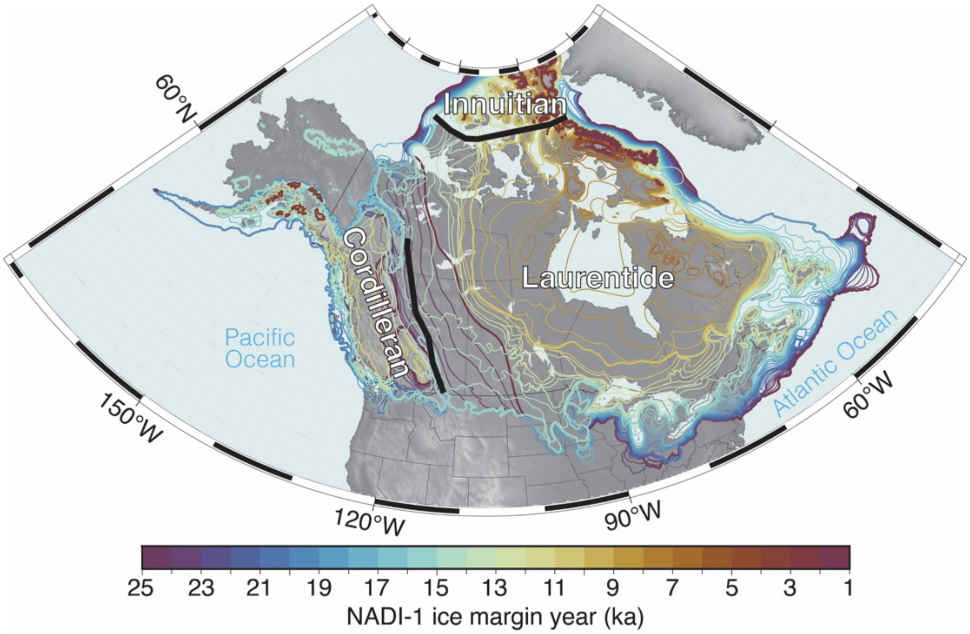

Figure 1. NADI-1 margins. NADI-1 margins (Dalton et al., 2023) from 25 ka through 1 ka at 1 ka intervals. The Laurentide, Cordilleran, and Innuitian ice sheet sectors of the North American Ice Sheet Complex are labeled. Margins at 25, 20, 15, 10, and 5 ka are plotted with bolder lines.

2 Methods

We generate North American Ice Sheet Complex ice sheet histories (a time series of ice sheet thickness reconstructions) using ICESHEET, a steady-state ice-sheet model that computes ice sheet thickness assuming perfectly plastic ice rheology (Gowan et al., 2016a). ICESHEET does not have a regular grid and, instead, iteratively computes ice thickness along flowlines at regular intervals within prescribed ice sheet margins. We use 5 km flowline intervals throughout this study. By employing the ICESHEET model, we aim to provide the best approximation of North American ice sheet geometry constrained by empirically derived ice sheet margins, while acknowledging that our methodology produces a simplified ice sheet representation that cannot fully capture the complexity of North American ice dynamics. Outside of North America, the ICESHEET modeling

https://doi.org/10.5194/egusphere-2026-4374
Preprint. Discussion started: 29 July 2026

approach has been previously employed to reconstruct the Eurasian ice sheet (Bradley et al., 2023; Pollard et al., 2023). Henceforth, we refer to our ice sheet thickness reconstructions simply as "ice sheet reconstructions" or "reconstructions".

To compute ice sheet geometry at a given time of interest, ICESHEET requires three inputs, including (1) prescribed ice-margins, (2) a basal shear stress map, and (3) regional topography. Because regional topography evolves over time due to GIA, ICESHEET was iterated twice to account for changes in bedrock topography. In the following, we provide further detail on each of the inputs used to generate the ice sheet reconstructions.

2.1 Ice margins from NADI-1

The ICESHEET modeling approach is time-independent: the model takes a prescribed ice margin at a given time as input and produces a single ice geometry for that time as output. We produce ice sheet thickness reconstructions (ICE-NADI-1, ICE-NADI-1_min, and ICE-NADI-1_max) using the NADI-1 optimal, minimum, and maximum isochrones, respectively, thus capturing the full range of uncertainty associated with NADI-1 margins (Dalton et al., 2023). The minimum and maximum NADI-1 margins represent end-member possibilities for North America ice margins, as they are based on combining minimum or maximum scenarios from all individual regions (Dalton et al., 2023). Thus, our ICE-NADI-1_min, and ICE-NADI-1_max can be considered end-member ice thickness reconstructions.

2.2 Basal shear stress

We adopt the same basal shear stress maps used in Gowan et al. (2016b) for North America, which were based on partitioning northern North America into sub-regions based on geological age and compositions and adjusting the shear stress estimates of Fisher et al. (1985) to fit GIA observations. Changing the basal shear stress values acts to either increase or decrease the basal friction, subsequently altering the ice surface slope and ice thickness. For example, an increase in basal shear stress will result in a thicker ice sheet. Following Gowan et al. (2016b), basal shear stress values generally decrease from their LGM values as deglaciation progresses.

2.3 GIA modeling to compute topography and relative sea-level changes

We adopt a global 1-D glacial isostatic adjustment (GIA) model to compute relative sea level (RSL) and paleotopography changes. The GIA model solves the sea-level equation up to spherical harmonic degree and order 512 following the pseudo-spectral implementation (Kendall et al., 2005), accounting for evolving shorelines and the migration of grounded, marine-based ice (Johnston, 1993; Milne et al., 1999; Lambeck et al., 2003; Kendall et al., 2005). A global ice sheet model is required in the GIA model, and we embed our North American reconstructions into the ICE-6G_C global ice sheet model (Peltier et al., 2015).

https://doi.org/10.5194/egusphere-2026-4374
Preprint. Discussion started: 29 July 2026

GIA simulations are carried out on a radially-varying, self-gravitating, elastically compressible Maxwell viscoelastic Earth. Elastic and density structure is adopted from the Preliminary Reference Earth Model (PREM: Dziewonski & Anderson, 1981). The predicted topography changes are input into the ICESHEET model for two iterations. To capture a wide range of possible lithospheric thickness and mantle viscosities appropriate for North America, we adopt four different viscoelastic Earth models (Earth_1, Earth_2, Earth_3, Earth_4; Table 1) in our GIA simulations with the NADI-1 optimal margins. We only generate ice sheet reconstructions with the NADI-1 minimum and maximum margins using the Earth_1 and Earth_2 models. Throughout, we primarily present and discussion reconstructions developed using the Earth_1 model. In all of the Earth models, the upper mantle extends from the base of the lithosphere to 670 km depth and the lower mantle extends from 670 km depth to the core-mantle boundary at 2,886 km depth.

Table 1. Summary of Earth models and ice margins used in the North American Ice Sheet Complex reconstructions.

	Earth_1	Earth_2	Earth_3	Earth_4
Lithospheric thickness (km)	96	70	120	48
Upper mantle viscosity (Pa s)	$3x10^{20}$	$2x10^{20}$	$4x10^{20}$	$2x10^{20}$
Lower mantle viscosity (Pa s)	10^{21}	10^{22}	10^{22}	$5x10^{21}$
ICE-NADI-1	Yes	Yes	Yes	Yes
ICE-NADI-1_min	Yes	Yes	No	No
ICE-NADI-1_max	Yes	Yes	No	No

The Earth_1, Earth_2, and Earth_3 models were previously adopted by Parang et al. (2024), Gomez et al. (2015), and Gowan et al. (2016b), respectively, to model GIA in North America. The Earth_1, Earth_2, and Earth_3 models span a range of viscoelastic Earth structures inferred for North America from analyses of ice-age datasets and geodetic observations, with lithospheric thicknesses ranging from 70-120 km, upper mantle viscosities ranging from $2x10^{20}$ to $4x10^{20}$ Pa s, and lower mantle viscosities ranging from 10^{21} to 10^{22} Pa s (Table 1; Mitrovica & Forte, 2004; Lambeck et al., 2014; Tarasov et al., 2012; Peltier et al., 2015; Roy & Peltier, 2015, 2018). We also consider a fourth Earth model, Earth_4, featuring a lithospheric thickness of 48 km, to evaluate how accounting for thinner lithosphere found in parts of North America, such as the Pacific coast (e.g., Afonso et al., 2019; Marsman et al., 2021; Yousefi et al., 2018) impacts the ice sheet reconstructions (Table 1). We adopt the Earth_1 model for our RSL predictions because Parang et al. (2024) identified it as the optimal viscoelastic Earth model for fitting RSL observations in eastern North America.

Throughout, we discuss the global mean sea level (GMSL) and sea-level equivalent (SLE) of our new reconstructions and previous reconstructions. Global mean sea level (GMSL) is defined as the global mean sea-level change produced by ice melt,

https://doi.org/10.5194/egusphere-2026-4374
Preprint. Discussion started: 29 July 2026

accounting for migrating shorelines. Ice volume is presented in units of sea-level equivalent (SLE), which is defined as the global mean sea-level change produced by evenly distributing the ice volume across the modern-day ocean area.

3 Results & Discussion

In the following, we provide a detailed description of ice thickness evolution across different sectors of the North American Ice Sheet Complex (Laurentide, Cordilleran, Innuitian). Adopting the NADI-1 optimal, minimum, and maximum margins in the ICESHEET modeling approach produces substantially different reconstructions (Figs. 2-3). We consider how our reconstructions inform North American ice volume evolution, global sea-level contributions, and relative sea-level observations over the deglaciation, noting differences between the ICE-NADI-1 reconstructions and existing reconstructions (i.e., ICE-7G, LW-6, NAICE). Finally, we describe how uncertainties in the ice sheet reconstructions propagate into uncertainties in paleotopography and present-day vertical crustal motion predictions for North America.

3.1 North American Ice Sheet Complex thickness evolution

Our optimal ICE-NADI-1 reconstruction contains a maximum total North American Ice Sheet Complex (Laurentide, Cordilleran, Innuitian) ice volume of 64 m SLE at 20 ka. Figure 4 shows ice sheet volume evolution over the deglaciation, for the entire North American Ice Sheet Complex as well as for the Laurentide, Cordilleran, and Innuitian sectors.

3.1.1 Laurentide Ice Sheet thickness evolution

From 25 ka to 22 ka, Laurentide Ice Sheet volume increases from 43 m SLE to its maximum volume of 53 m SLE in the ICE-NADI-1 reconstruction (Fig. 4c). Laurentide Ice Sheet volume then gradually decreases from 22 to 17.5 ka, after which ice loss accelerates as ice margin retreat progresses (Figs. 2-3, 4c).

The Laurentide Ice Sheet is multi-domed in all three ICE-NADI-1 reconstructions, with one dome centered east of the Great Slave Lake (Keewatin Dome), a second dome centered east of James Bay (Québec-Labrador Dome), and a third dome centered south of Baffin Island (Foxe Dome) (Figs. 2-3, S1-S3). The Keewatin Dome is the thickest of the three Laurentide ice domes from 25 to 15 ka in the ICE-NADI-1 reconstruction, reaching a maximum thickness of ~4,040 m between 22 and 16.5 ka (Figs. 2a-e, 3a-b, S1-S2). The Keewatin Dome reaches its maximum thickness when the ice saddle connects the Laurentide Ice Sheet with the Cordilleran Ice Sheet (Figs. 2d-f, S1-S2). As soon as saddle collapse initiates at 16 ka, the Keewatin Dome starts thinning (Fig. 3a-b).

https://doi.org/10.5194/egusphere-2026-4374
Preprint. Discussion started: 29 July 2026

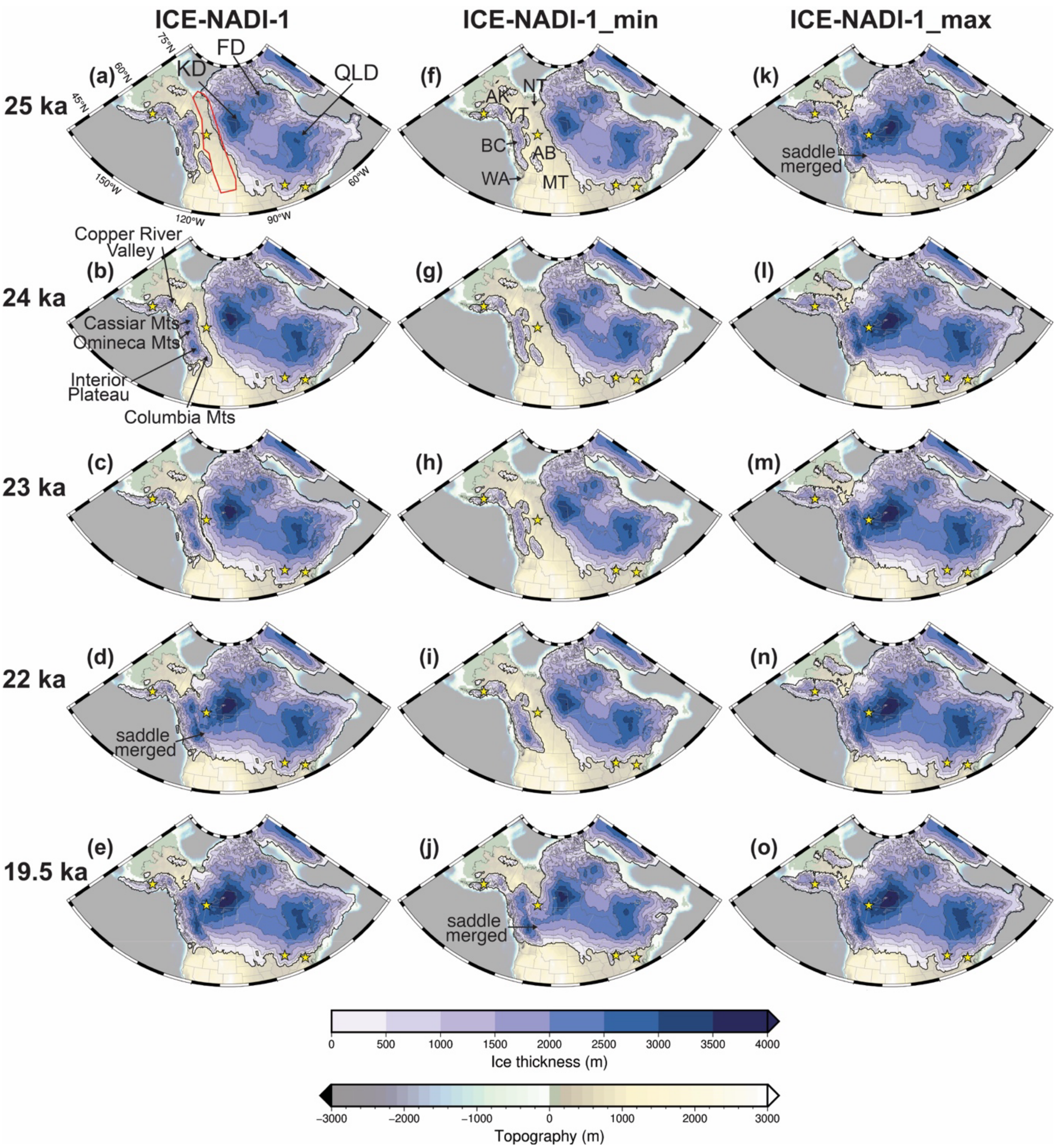

Figure 2. ICE-NADI-1 reconstructions of North American Ice Sheet Complex advance to Last Glacial Maximum extent. (a-f) ICE-NADI-1 (optimal), (g-l) ICE-NADI-1_min, and (m-r) ICE-NADI-1_max ice sheet thickness reconstructions at 25 ka, 24 ka, 23 ka, 22 ka, and 19.5 ka. All reconstructions shown are associated with the Earth_1 model. Paleotopography is plotted beneath the ICE-NADI-1 reconstruction for each time interval. Modern-day coastlines and state/provincial boundaries are plotted for reference. Specific states and provinces are labeled, including Washington (WA), Montana (MT), Alaska (AK), British Columbia (BC), Alberta (AB), the Yukon (YT), and the Northwest Territories (NT). Ice domes discussed in the text are also labeled: KD: Keewatin Dome, FD: Foxe Dome, QLD: Québec-Labrador Dome. Geographic locations and mountain ranges discussed in the text are labeled. Yellow stars mark the locations of the paleotopography time series shown in Fig. 9g-j. The red polygon in (a) marks the location of the Laurentide – Cordilleran saddle region discussed throughout.

https://doi.org/10.5194/egusphere-2026-4374
Preprint. Discussion started: 29 July 2026

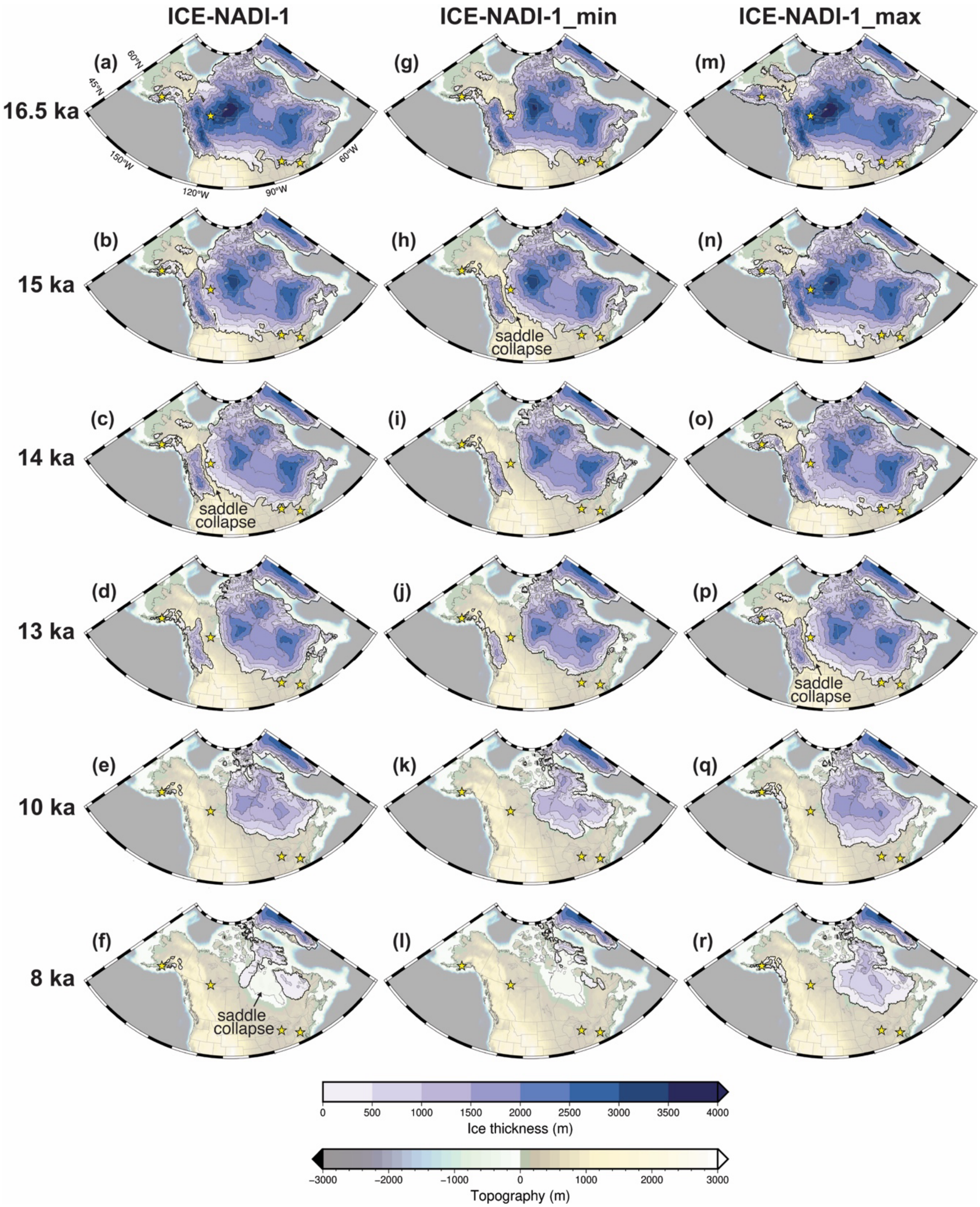

Figure 3. ICE-NADI-1 reconstructions for the deglaciation of the North American Ice Sheet Complex. (a-f) ICE-NADI-1, (g-l) ICE-NADI-1_min, and (m-r) ICE-NADI-1_max reconstructions at 16.5 ka, 15 ka, 14 ka, 13 ka, 10 ka, and 8 ka. All reconstructions shown use the Earth_1 model. Yellow stars mark the locations of the paleotopography time series shown in Fig. 9g-j.

https://doi.org/10.5194/egusphere-2026-4374
Preprint. Discussion started: 29 July 2026

The Québec-Labrador ice dome is the second largest ice dome of the Laurentide Ice Sheet. The maximum thickness of the Québec-Labrador ice dome hovers around ~3,190 m from 25 to 15 ka in the ICE-NADI-1 reconstruction (Figs. 2a-e, 3a-b, S1-S2). At 14 ka, after the Laurentide-Cordilleran saddle collapse, the Québec-Labrador ice dome overtakes the Keewatin Dome as the thickest ice dome of the Laurentide Ice Sheet (Fig. 3c). At this time, the Québec-Labrador Dome is up to 3,050 m thick whereas the Keewatin Dome has a maximum thickness of 2,850 m. From 14 ka through 10 ka, the maximum thickness of the Québec-Labrador and Keewatin ice domes both decrease but remain comparable in thickness (Figs. 3c-e, S2-S3).

The Foxe Dome is the smallest of the three Laurentide Ice Sheet domes (Figs. 2-3). From 25 to 14.5 ka, the maximum thickness of the Foxe Dome hovers around 2,800 m (Figs. 2a-e, 3a-c, S2-S3). After 12 ka, the Foxe Dome starts thinning rapidly as deglaciation proceeds and the ice margins retreat, culminating with the collapse of the dome around 8 ka (Figs. 3e, S2-S3).

3.1.2 Cordilleran Ice Sheet thickness evolution

At its maximum extent in the NADI-1 margins (Dalton et al., 2023), the Cordilleran Ice Sheet spanned from the Alaska Peninsula across south-central and southeastern Alaska and extended south through British Columbia into northern Washington and western Montana (Fig. 2). From 25 ka to 19.5 ka, the volume of the Cordilleran Ice Sheet increases from 3.5 m SLE to near its maximum volume of 7.7 m SLE in the ICE-NADI-1 reconstruction (Fig. 4d). Note, when computing the volume of the Cordilleran Ice Sheet, we include all ice in the Alaska Peninsula, south-central, and southeastern Alaska along with ice in British Columbia, the Yukon, and the northwestern United States. The volume of the Cordilleran Ice Sheet briefly sits around ~7.7 m SLE from 19.5 to 18.5 ka in ICE-NADI-1, after which the volume decreases as the deglaciation proceeds (Figs. 2-3, 4d, S2-S3).

In our ICE-NADI-1 Cordilleran reconstructions, the thickest and highest elevation ice stretches from the Columbia Mountains in British Columbia north across the Interior Plateau and into the Omineca Mountains and Cassiar Mountains (Figs. 2-3, S1-S2). At its maximum extent, the Cordilleran Ice Sheet has two main ice domes, one located in the Interior Plateau and a second located in the Cassiar Mountains near the British Columbia-Yukon border. The Interior Plateau Dome reaches its maximum thickness of ~3,400 m from 19 to 18.5 ka in the ICE-NADI-1 reconstruction (Figs. 2e, S1). Like the Interior Plateau Dome, the Cassiar Mountains Dome also reaches its maximum thickness of ~3,350 m at 19 ka; however, it maintains this peak thickness until 16.5 ka – 2 kyr longer than it does at the Interior Plateau Dome (Figs. 2e, S1-S2).

Ice thicknesses remain below 1,500 m across much of southeastern and south-central Alaska, as well as in the Alaska Peninsula, in all three of the ICE-NADI-1 reconstructions (Figs. 2-3). Across Alaska as a whole, ice is thickest in the Copper River Valley, reaching ~2,100 m at 23 ka in the ICE-NADI-1 reconstruction (Figs. 2c, S1). Notable discrepancies are found amongst the

ICE-NADI-1, ICE-NADI-1_min, and ICE-NADI-1_max reconstructions in the Bering Sea around the Alaska Peninsula (Figs. 2-3). For example, in the ICE-NADI-1_max reconstruction, the ice margin extends into the southeastern Bering Sea from 25 ka to 16.5 ka, resulting in an ice dome up to ~2,100 m thick centered at the eastern end of the Alaska Peninsula (Fig. 2k-o). A comparable ice dome is absent in the ICE-NADI-1 and ICE-NADI-1_min reconstructions because the NADI-1 ice margin (Dalton et al., 2023) does not extend into the Bering Sea in either of these reconstructions (Figs. 2a-j, 3g).

3.1.3 Innuitian Ice Sheet

The Innuitian Ice Sheet reached its maximum volume of 2.5 m SLE at 25 ka in our ICE-NADI-1 reconstruction (Fig. 4e). From 25 to 15.5 ka, the Innuitian lost ice volume at an average rate of 0.05 mm/year SLE. Ice loss accelerated around 15 ka, increasing to an average rate of 0.2 mm/year SLE. The timing of this acceleration in ice loss coincides with the start of the Innuitian evolving from a singular cohesive ice mass into a series of smaller ice masses, each centered on an Arctic island (NADI-1; Dalton et al., 2023) (Figs. 3, S3). By 8 ka, the ice sheet volume is diminished to 0.15 m SLE in the ICE-NADI-1 reconstruction, after which its volume declined gradually to present. The Innuitian Ice Sheet is thickest from 25 to 19 ka in our ICE-NADI-1 reconstruction, reaching a maximum thickness of ~1,700 m (Figs. 2-3).

3.2 Ice margin treatment informs ice volume evolution and sea-level contributions

We can gain insight into ice volume evolution from our new North American ice sheet reconstructions. Because our ice sheet reconstructions assign ice thicknesses by enforcing empirically derived ice margins with relatively simple ice sheet physics, we can explore how adopting different 2-D ice margins impacts the 3-D evolution of ice volume (Fig. 2-5). Our ICE-NADI-1 reconstructions capture large fluctuations in North American ice volume connected to key moments in ice margin evolution, such as lowering GMSL across the LGM during saddle merging and ice thinning dynamics associated with saddle collapses. We compare ice volume evolution among the three new ICE-NADI-1 reconstructions as well as to existing reconstructions, including ICE-7G (Roy & Peltier, 2017), LW-6 (Lambeck et al., 2017), and NAICE (Gowan et al., 2016b). We note here that geologic and geodetic observations were used to tune the ICE-7G, LW-6, and NAICE reconstructions and, in contrast, we do not tune the ICE-NADI-1 reconstructions. More specifically, ICE-7G is tuned using RSL observations and GNSS observations of vertical crustal motion (Roy & Peltier, 2017). LW-6 and NAICE are constrained by RSL and GNSS observations, in addition to glacial lake tilt observations (Lambeck et al., 2017; Gowan et al., 2016b).

3.2.1 North American contribution to global ice volume during the Last Glacial Maximum

Our optimal ICE-NADI-1 reconstruction contains a maximum total North America ice volume of 64 m SLE at 20 ka, approximately 20-25% smaller than the 79 m and 84 m SLE contained in LW-6 and ICE-7G reconstructions, respectively (Fig. 4b). In contrast, our total North American ice volume is slightly larger (5 m SLE) than that contained in NAICE (59 m SLE), which was similarly constructed using the ICESHEET model. The maximum ice volume contained in North America varies by >20 m SLE between ICE-NADI-1_min (51 m SLE at 18.5 ka) and ICE-NADI-1_max (71 m SLE at 20 ka). This ice volume

https://doi.org/10.5194/egusphere-2026-4374
Preprint. Discussion started: 29 July 2026

difference is greater than that resulting from reconstructions adopting different Earth models (<1 m SLE) (Fig. 4b, Text S1). The timing of peak ice volume in the ICE-NADI-1 reconstructions varies between 20 ka (ICE-NADI-1_max) and 18.5 ka (ICE-NADI-1_min) (Fig. 4b). In contrast, ICE-7G and LW-6 both reach their maximum ice volumes much earlier, at 25 ka.

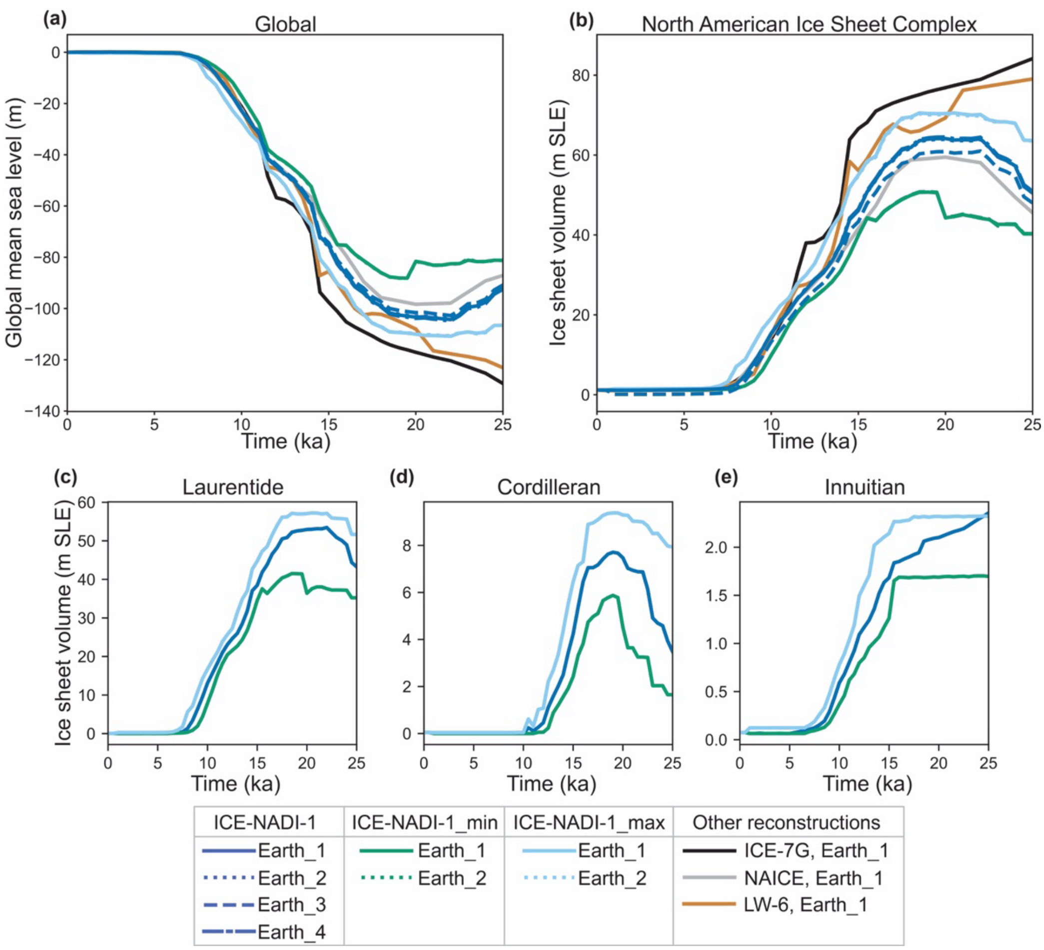

Figure 4. Global mean sea level and ice volume. (a) Global mean sea-level (GMSL) history for the ICE-NADI-1 (dark blue), ICE-NADI-1_min (green), and ICE-NADI-1_max (light blue) reconstructions plotted alongside the ICE-7G (black), NAICE (gray), and LW-6 (brown) reconstructions. The ICE-NADI-1, NAICE, and LW-6 reconstructions are all embedded into the ICE-6G_C global reconstruction (Peltier et al., 2015); therefore, all discrepancies in GMSL amongst the reconstructions arises from ice sheet geometry differences in North America. (b) Ice volume for North America. (c-e) Ice volume from the ICE-NADI-1 ICE-NADI-1_min, and ICE-NADI-1_max reconstructions with Earth_1 for the (c) Laurentide, (d) Cordilleran, and (e) Innuitian ice sheets.

Our ICE-NADI-1 reconstruction, which includes the North American ice history patched into the ICE-6G_C ice history (Peltier et al., 2015) to build a global ice history, contains a GMSL lowstand of -104 m at 22 ka (Fig. 4a; 88 m GMSL at 19.5 ka for ICE-NADI-1_min, -111 m GMSL at 22 ka for ICE-NADI-1_max). In contrast, ICE-7G has a sea-level lowstand of -133 m GMSL at 26 ka (Fig. 4a). LW-6 and NAICE have LGM sea-level lowstands of -123 m GMSL (25 ka) and -98 m

https://doi.org/10.5194/egusphere-2026-4374
Preprint. Discussion started: 29 July 2026

GMSL (20 ka), respectively (Fig. 4a). Since the ICE-NADI-1, LW-6, and NAICE reconstructions are all embedded into the ICE-6G_C global reconstruction, discrepancies in GMSL amongst these reconstructions arise exclusively from ice sheet geometry differences in North America.

While constraints on LGM sea level remain sparse, RSL observations indicate a GMSL lowstand of ~-135 to -120 m from ~26-19 ka (Yokoyama et al., 2000, 2018; Hanebuth et al., 2000; Peltier & Fairbanks, 2006; Austermann et al., 2013; Ishiwa et al., 2016). Recent studies suggest that LGM GMSL stayed near -100 m (Vacchi et al., 2025) to -110 m (Vacchi et al., 2025; Yokoyama et al., 2018), except for a short-lived GMSL lowstand (<4 ky) of -130 to -125 m (Yokoyama et al., 2018). Our ICE-NADI-1 reconstruction, with a minimum GMSL of -104 m, is consistent with the -100 to -110 m that might have characterized the majority duration of the LGM, and it is possible our reconstruction would not capture the minimum global lowstand if the brief drop in GMSL to ~-130 m was driven by growth of another ice sheet, as hypothesized in Yokoyama et al. (2018).

RSL observations from the Indo-Pacific Ocean indicate up to ~20 m GMSL fall from ~26 to 20 ka, with GMSL reaching its minimum near the end of the LGM at ~20.5 ka (Yokoyama et al., 2018; Ishiwa et al., 2016). Falling GMSL during the LGM has been attributed to the southward advance of the Laurentide Ice Sheet and expansion of the Scandinavian Ice Sheet (Lambeck et al., 2014). However, neither the ICE-7G or LW-6 reconstructions capture GMSL fall from ~26-20 ka, instead they show ~15 m and ~13 m of GMSL rise, respectively (Fig. 4a). In contrast, North American ice sheet growth (corresponding to ~11 m of GMSL fall) occurs in our ICE-NADI-1 reconstruction from 25 to 20 ka (Fig. 4a-b). While Laurentide southward advance does contribute to North American ice volume growth in ICE-NADI-1 (up to 0.4 m SLE from 25-20 ka), the formation of the saddle between the Laurentide and Cordilleran ice sheets during this period drives a greater increase in North American ice volume (Fig. 2a-e). Saddle growth causes widespread thickening across the Laurentide and Cordilleran ice sheets, leading to 5.3 m SLE of ice growth in the saddle region itself and 4 m SLE of ice growth across the Cordilleran Ice Sheet (Figs. 2d, 4). Thus, the development and merging of the Laurentide-Cordilleran ice saddle is a larger contributor to GMSL fall during the LGM than southern Laurentide ice advance.

3.2.2 Timing of ice saddle collapse determines history of sea-level contributions

Geological evidence suggests the Laurentide – Cordilleran saddle unzipped between 14.5 and 14 ka (NADI-1; Dalton et al., 2023), and our ICE-NADI-1 ice sheet thickness reconstruction produces 6.3 m SLE of ice melt from North American during this period (Figs. 2, 4). Collapse of the saddle connecting the Laurentide and Cordilleran ice sheets has previously been identified as a major contributor to Meltwater Pulse 1a (MWP-1a), a period of ~15-20 m of global sea-level rise from ~14.5-14 ka (Deschamps et al., 2012; Lin et al., 2021). From an ensemble of North American deglaciation simulations, Gregoire et al. (2016) finds that Laurentide-Cordilleran saddle collapse triggers a North American contribution ranging from 3 to 11 m GMSL in 340 years. Thus, in the ICE-NADI-1 reconstruction, the North American contribution to sea-level rise during MWP-

https://doi.org/10.5194/egusphere-2026-4374
Preprint. Discussion started: 29 July 2026

1a falls within the GMSL range estimated by Gregoire et al. (2016) and is, furthermore, consistent with recent studies based on geological records (Stoker et al., 2022; Norris et al., 2022; Reyes et al., 2024) and fingerprinting analyses (Lin et al., 2021; Coonin et al., 2025) that place the North American MWP-1a contribution between 3 and 15 m GMSL. Still, we highlight that there is uncertainty associated with the timing of Laurentide – Cordilleran saddle collapse in the NADI-1 margins by Dalton et al. (2023). While Laurentide – Cordilleran saddle collapse happens during MWP-1a in the NADI-1 optimal margins, saddle collapse occurs either before or after MWP-1a in the NADI-1 minimum (15 ka) and NADI-1 maximum (13 ka) margins, respectively (Fig. 3).

From 14.5-14 ka, 5.3 m SLE is lost from the Laurentide Ice Sheet while 0.9 m SLE is lost from the Cordilleran Ice Sheet in ICE-NADI-1 (Fig. 4). The saddle region (Fig. 2a) alone loses only 1.5 m SLE from 14.5 to 14 ka. Thus, the collapse of the Laurentide-Cordilleran saddle itself does not drive the most substantial North American sea-level contribution to MWP-1a. Instead, the widespread thinning across the Laurentide and, to a lesser degree, the Cordilleran, that is triggered by saddle collapse drives a large part of the North American contribution to global sea-level rise during this period. Our reconstruction captures ice thinning after saddle collapse because our method enforces physically-realistic, equilibrium ice thickness profiles. Therefore, saddle collapse produces a series of ice domes, which contain substantially less ice volume than reconstruction methods with unrealistically-thick ice margins, like ICE-7G (Figs. 3-4).

Rates of ice volume change vary substantially among the new and existing reconstructions (Fig. 5). The ice loss rate at 14 ka in ICE-NADI-1 (13 mm SLE/year) is less than half the rate of ice loss in ICE-7G and LW-6 (~30 mm/year) (Fig. 5b). Thus, ICE-NADI-1 reconstruction suggests a smaller North American contribution to MWP-1a compared to ICE-7G and LW-6 (Fig. 5). A smaller North American contribution to MWP-1a permits a larger MWP-1a contribution from other ice sheets, such as the Eurasian Ice Sheet Complex (e.g., Brendryen et al., 2020; Lin et al., 2021; Coonin et al., 2025).

Instead of two large-magnitude meltwater pulses between ~14.5 and 9.2 ka, as in ICE-7G, ICE-NADI-1 has numerous, lower-magnitude ice melt pulses over this interval (Fig. 5). These multiple lower-magnitude ice melt pulses, particularly within the Laurentide sector, are more consistent with recent observations of four millennial-scale meltwater events in the Labrador Sea between 14 and 8.2 ka reported by You et al. (2023), as well as the 10.3 ka sea-level rise pulse identified by Hijma et al. (2025).

The ICE-NADI-1 reconstructions also capture the ice volume associated with the collapse of the Hudson Bay Ice Saddle. In ICE-NADI-1, North America undergoes 6.3 m SLE of ice melt from 9 to 7 ka, whereas ICE-NADI-1_max and ICE-NADI-1_min produce 10.2 and 1.9 m SLE of ice melt over the same interval, respectively (Fig. 4). Recently, Mukherjee et al. (2025) argued that North America ice melt from 9 to 7 ka must have produced ~14 m SLE of ice melt to satisfy RSL observations. Like previous reconstructions (ICE-7G, NAICE, LW-6), our optimal ICE-NADI-1 reconstruction indicates less ice melt from 9 to 7 ka, with larger amounts of melt occurring prior to 9 ka (10 m SLE melt from 10.5 to 9 ka). However, the ICE-NADI-

https://doi.org/10.5194/egusphere-2026-4374
Preprint. Discussion started: 29 July 2026

1_max reconstruction produces much higher ice melt from 9 to 7 ka (10.2 m SLE), which is consistent with the timing of the Mukherjee et al. (2025) RSL dataset. Hudson Bay Ice Saddle collapse occurs by 8 ka in the NADI-1 optimal margins (Gauthier et al., 2020; Dalton et al., 2023) whereas saddle collapse does not occur until 7 ka in NADI-1 maximum margins (Fig. S3). While Hudson Bay Saddle Collapse is generally thought to have occurred by 8 ka (Dyke, 2004; Gauthier et al., 2020; Dalton et al., 2023), uncertainty in the NADI-1 margins permit a later timing of saddle collapse (Fig. S3), which may be consistent with the Mukherjee et al. (2025) RSL dataset that requires substantial ice melt from 9 to 7 ka.

RSL records indicate that maximum Holocene rates of GMSL rise reached up to ~13 mm/year, with a background GMSL rate of ~1-2 mm/year (Hijma & Cohen, 2019; Rush et al., 2023; Hijma et al., 2025). Rates of GMSL rise from ICE-NADI-1 (<8 mm/yr) are more consistent with Holocene GMSL rates inferred from RSL observations than those predicted by ICE-7G (Hijma & Cohen, 2019; Rush et al., 2023; Hijma et al., 2025), as ICE-NADI-1 reduces the North American contribution (Fig. 5).

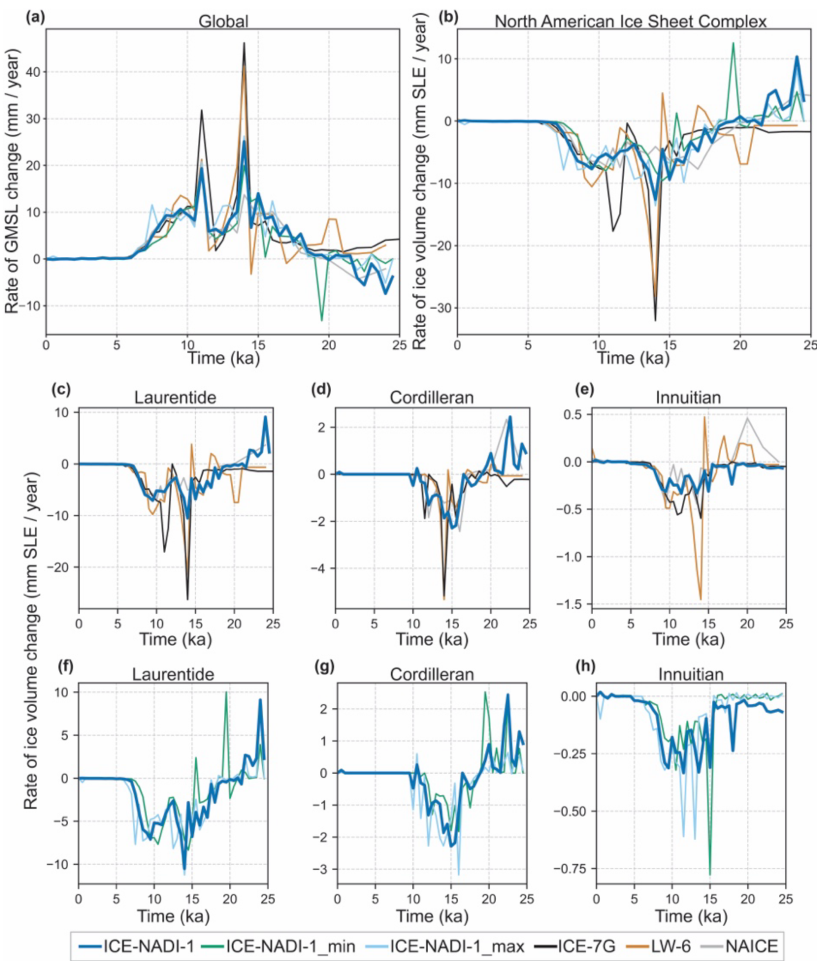

https://doi.org/10.5194/egusphere-2026-4374
Preprint. Discussion started: 29 July 2026

Figure 5. Rate of global mean sea-level change and ice volume change. (a) Rate of global mean sea-level (GMSL) change and (b) rate of North American Ice Sheet Complex ice volume change for the ICE-NADI-1, ICE-NADI-1_min ICE-NADI-1_max, ICE-7G, LW-6, and NAICE reconstructions, all with Earth_1. (c-d) Rate of ice volume change of the Laurentide, Cordilleran, and Innuitian ice sheet for the ICE-NADI-1, ICE-7G, LW-6, and NAICE reconstructions with Earth_1. (f-h) Same as (c-d) but for just ICE-NADI-1, ICE-NADI-1_min, and ICE-NADI-1_max reconstructions.

3.3 Fit to relative sea-level observations matches or outperforms previous reconstructions

To quantitatively evaluate our North American reconstructions, we compare RSL predictions from our GIA simulations with ICE-NADI-1, ICE-NADI-1_min, and ICE-NADI-1_max with three regional RSL compilations (Figs. 6-7, S4-S14). The regional RSL compilations include sea-level index points (SLIPs) and sea-level limiting points from the eastern Canadian coastline (Vacchi et al., 2018), the Atlantic coast of the United States (Engelhart & Horton, 2012), and the Pacific Coast of central North America (Engelhart et al., 2015) (Figs. 6-7, S4-S14). In Figs. 6-7, we show RSL data-model comparisons for a select subset of regions in the Vacchi et al. (2018) and Engelhart & Horton (2012) compilations. Data-model comparisons for all regions included in the two compilations as well as the Engelhart et al. (2015) compilation can be found in Figs. S4-S14. While we use all of the sea-level observations included in the Vacchi et al. (2018) and Engelhart & Horton (2012) compilations, we only use sea-level observations from regions 1-9 in the Engelhart et al. (2015) compilation (Figs. S4-S14), regions where no tectonic correction was applied in Yousefi et al. (2018).

To facilitate comparison of our new reconstructions with existing reconstructions, we plot our RSL predictions alongside those generated using the ICE-7G, LW-6, and NAICE reconstructions. All RSL predictions shown in Figs. 6-7 are produced using the Earth_1 model in the GIA modeling approach described in Section 2.3. We also present RSL predictions for the ICE-7G and NAICE reconstructions with the Earth_3 model in Figs. S4-S14, used in Gowan et al. (2016b) for NAICE and closely approximating the VM7 model associated with ICE-7G, which has average upper and lower mantle viscosities of 4.5×10^{20} Pa s and 7.45×10^{22} Pa s, respectively (Roy & Peltier, 2017). We find that in eastern Canada and the US Atlantic coast predicted relative sea level at 8 ka based on different ice sheet reconstructions can vary by more than 100 m (Fig. 6-7).

In this study, we do not tune our ice sheet reconstructions to fit RSL observations; therefore, we acknowledge that there will be a misfit between our model predictions and RSL observations. To assess the misfit between the RSL observations and RSL predicted using the new North American reconstructions, we compute the chi squared (χ^2) misfit using SLIPs:

$$\chi^2 = \frac{1}{(N-1)} \sum_{i=1}^{N} \left(\frac{(RSL_i^p - RSL_i^{obs}}{\sigma_i} \right)^2, \quad (1)$$

where RSL_i^p and RSL_i^{obs} are respectively the predicted and observed sea level at a given location and time, *i*. σ_i is the 2-sigma elevation error associated with RSL_i^{obs}, and N is the total number of SLIP observations. We compute the χ^2 misfit using SLIPs

https://doi.org/10.5194/egusphere-2026-4374
Preprint. Discussion started: 29 July 2026

(no limiting data) from all three of the North America sea-level compilations as well as for each of the compilations individually (Fig. 8).

All three ICE-NADI-1 reconstructions with the Earth_1 model outperform the ICE-7G and NAICE reconstructions using the associated Earth_3 viscoelastic model (Fig. 8). When all three North American RSL compilations are considered together, the NAICE reconstruction with the Earth_1 viscoelastic model yields the lowest χ^2 misfit, with the ICE-NADI-1 reconstruction performing comparably, with only a modestly higher misfit (χ^2 = 36 vs 38; Fig. 8). Regionally, NAICE produces the lowest data-model misfit for eastern North America, with ICE-NADI-1 reconstruction performing comparably. The ICE-NADI-1_min reconstruction has the lowest data-model misfit for the Pacific Coast of central North America. Broadly, our χ^2 misfit values underscore the large misfits between current GIA predictions and RSL observations that must be reconciled before we can build a refined understanding of the history of ice sheet loading and Earth structure across North America.

https://doi.org/10.5194/egusphere-2026-4374
Preprint. Discussion started: 29 July 2026

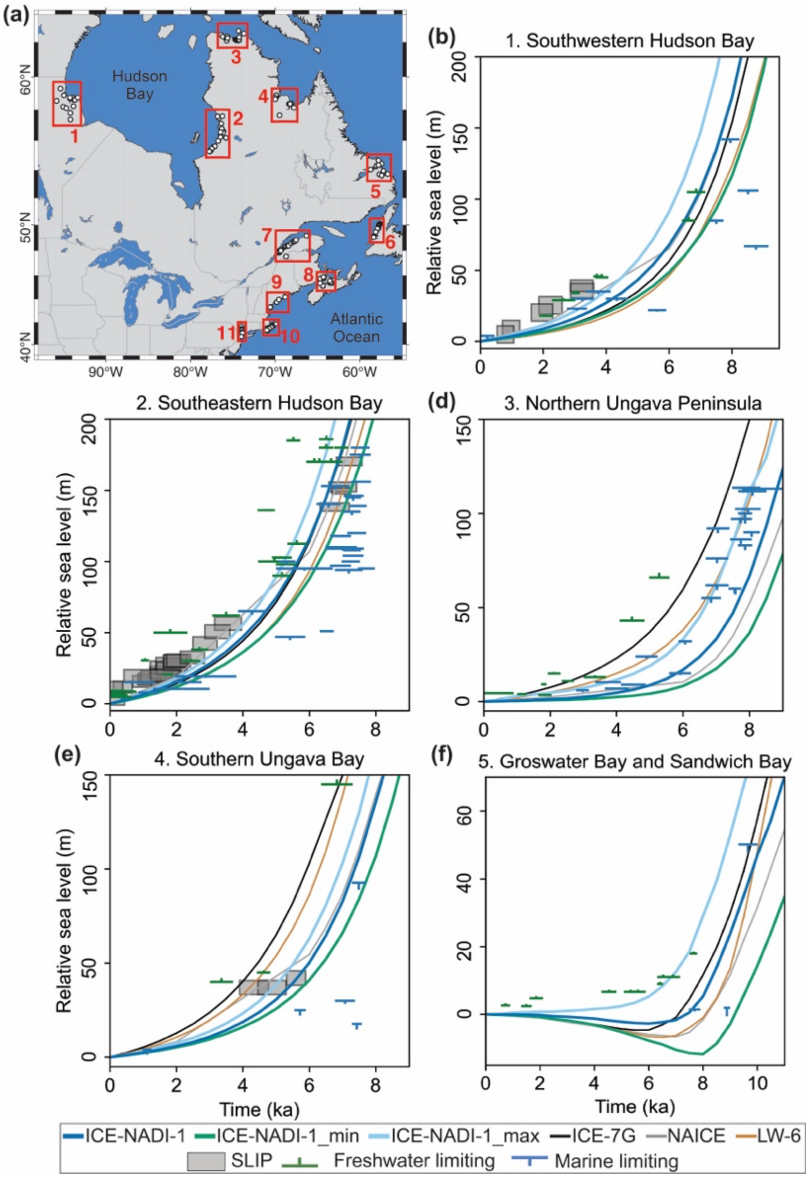

Figure 6. Data-model comparison along the eastern North American coastline. (a) Map showing the spatial distribution of selected relative sea-level (RSL) data from the Vacchi et al. (2018) and Engelhart & Horton (2012) compilations for regions 1-11. White circles mark the locations of individual RSL observations. (b-f) Data-model comparisons for regions 1, 2, 3, 4, and 5 shown in (a). Data-model comparisons for the other regions shown in (a) are plotted in Fig. 7. The Earth_1 model is used for all RSL predictions in this figure and Fig. 7.

https://doi.org/10.5194/egusphere-2026-4374
Preprint. Discussion started: 29 July 2026

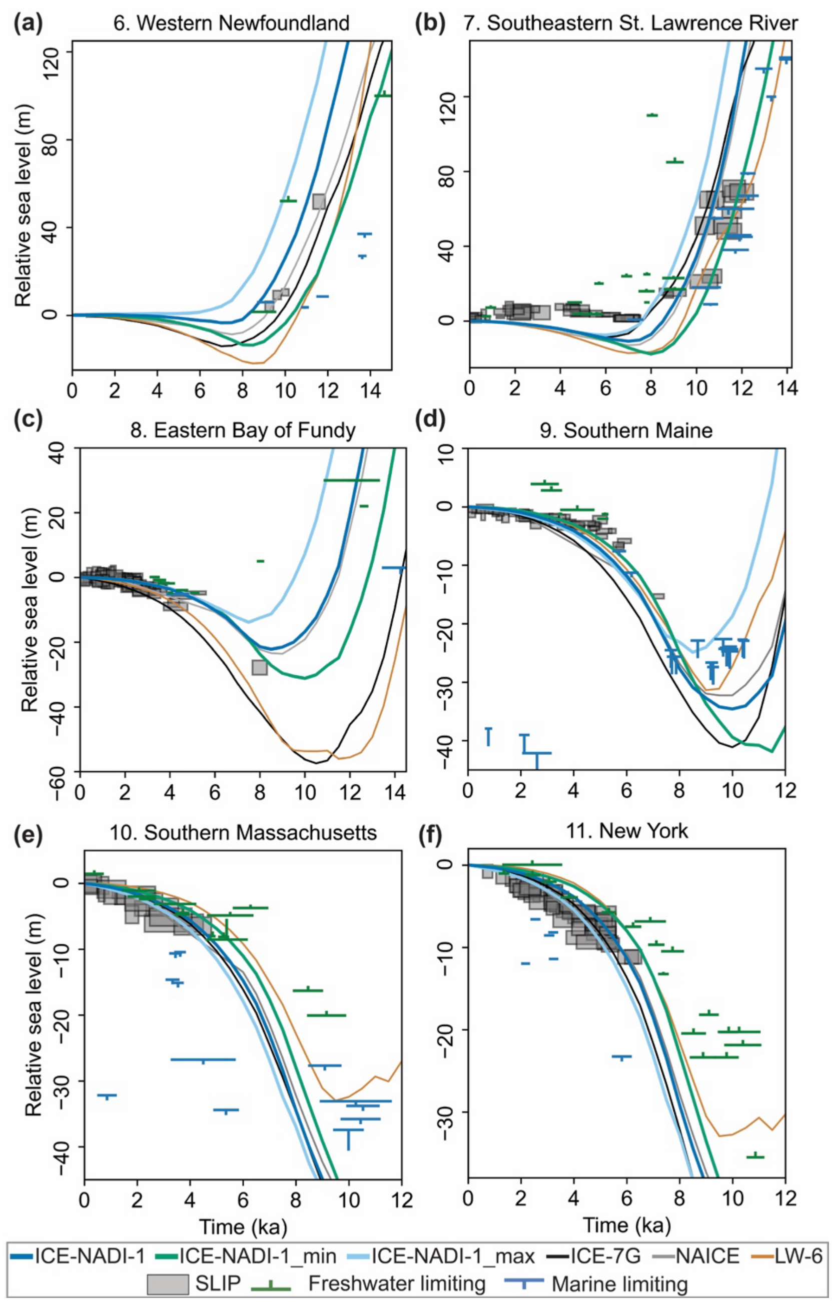

Figure 7. Data-model comparison along the eastern North American coastline continued. Data-model comparison for regions 6-11 from Fig. 6a along the eastern North American coastline. See the caption of Fig. 6 for additional details.

https://doi.org/10.5194/egusphere-2026-4374
Preprint. Discussion started: 29 July 2026

	All compilations (N=1271)	Eastern Canadian coastline (N=404)	Atlantic coast of United States (N=492)	Pacific coast of central North America (N=375)
ICE-NADI-1 Earth_1	38	27	21	71
ICE-NADI-1_min Earth_1	41	40	21	66
ICE-NADI-1_max Earth_1	47	47	24	78
ICE-7G Earth_1	50	38	32	85
NAICE Earth_1	36	24	20	70
LW-6 Earth_1	77	107	20	95
ICE-7G Earth_3	89	140	36	109
NAICE Earth_3	91	142	46	87
LW-6 Earth_3	54	41	50	76

Figure 8. Fit to relative sea-level observations. χ^2 misfit values for all three North American sea-level compilations and for each regional compilation individually. We compute χ^2 misfit values for ICE-NADI-1 reconstructions with the Earth_1 model. We compute χ^2 misfit values for the ICE-7G, NAICE, and LW-6 reconstructions using both the Earth_1 and Earth_3 models.

3.4 Ice margin bounds allow uncertainty quantification in GIA predictions

Currently, quantifying GIA prediction uncertainty associated with ice loading history is challenging. Despite the ubiquity of using GIA models to interpret relative sea-level observations and geodetic data (e.g., Simon et al., 2016, 2017; Love et al., 2016; Yousefi et al., 2018; Caron et al., 2018; Li et al., 2020; Austermann et al., 2021; Parang et al., 2024), it remains unclear how much uncertainty in GIA predictions stems from our imperfect knowledge of the ice loading history versus Earth structure (e.g., Melini & Spada, 2019; Li et al., 2020). Previous studies have quantified uncertainty related to Earth structure by performing simulations with a range of Earth structure parameters (e.g., Caron et al., 2018; Melini & Spada, 2019; Li et al., 2020); however, published ice histories do not contain maximum and minimum bounds that permit uncertainty quantification.

Can representing the full range of plausible ice margins allow us to quantify uncertainty in GIA predictions? In the following, we use our ICE-NADI-1, ICE-NADI-1_min, and ICE-NADI-1_max reconstructions to quantitatively assess how unknowns in empirically derived ice margins propagate to uncertainty in ice sheet thickness and, subsequently uncertainty in RSL, paleotopography, and present-day vertical crustal motion predictions for North America.

3.4.1 Relative sea level

We find up to ~10-40 m difference in RSL predictions from 20 to 2 ka arises from variability among the ICE-NADI-1, ICE-NADI-1_min and ICE-NADI-1_max reconstructions (Figs. 6-8, S4-S14, Text S2). Thus, uncertainties in RSL predictions (~10-40 m) associated with ice geometry are comparable to those associated with different Earth structure realizations (up to ~20-45 m between 15-11 ka; Li et al., 2020). This outcome is not surprising given that some areas of ice retreat show uncertainties in the range of 100s of km for a given time slice, primarily driven by geochronological uncertainty (Dalton et al., 2023). Because these uncertainties were not part of the earlier reconstructions of North American ice extent by Dyke (2004), previous GIA modeling studies fail to capture the full range of possible North American ice margin extents over the deglaciation (e.g., Love et al., 2016; Simon et al., 2016; Roy & Peltier, 2017; Yousefi et al., 2018; Parang et al., 2024; Williams et al., 2024) as well as those that incorporate variations of that margin chronology (e.g., GLAC1D; Tarasov et al., 2012). Thus, past GIA modeling studies are likely incapable of capturing the full spectrum of plausible RSL variability, which may bias studies that minimize RSL data-model misfits to infer lithospheric thickness and mantle viscosity.

3.4.2 Paleotopography

Similarly, our ICE-NADI-1 reconstructions span a range of crustal deformation magnitudes and patterns across the maximum and minimum scenarios (Fig. 9). Bounds on empirical ice margins also allow uncertainty quantification on paleotopography (defined as the negative of relative sea level) reconstructions over the last deglaciation. Such predictions are key for studies of past landscapes or glacial lake shoreline tilts, or any case where it would be useful to know the history of subsidence or uplift (e.g., Austermann et al., 2020, 2022; Kodama et al., 2023; Sanborn et al., 2025). Figure 9 shows how much North American paleotopography predictions vary among GIA simulations that adopt different North American ice sheet reconstructions. We find the largest magnitude discrepancies in paleotopography predictions in western Canada, where differences among the ICE-NADI-1, ICE-NADI-1_max, and ICE-NADI-1_min reconstructions reach up to ~500 m, even predicting opposite-signs, in part, due to variability in in the timing of ice saddle formation (Fig. 9a-f). More specifically, we find major differences in paleotopography predictions at the British Columbia, Northwest Territories, and Alberta (BC, NT, AB) border intersection, a region that lies where the Laurentide and Cordilleran ice sheets were connected by an ice saddle (Figs. 2-3). From 25 ka to ~8 ka, paleotopography in this region is controlled by the solid Earth's response to the growth and collapse of the ice saddle (Fig. 9). The BC, NT, AB border intersection undergoes ~600 m of subsidence from 25 to 16 ka as the Laurentide – Cordilleran saddle grows in the ICE-NADI-1 GIA simulation (Fig. 9h). Consistent with the delayed saddle merging and more rapid collapse, subsidence is much more subdued in the ICE-NADI-1_min GIA simulation, reaching up to only ~130 m at the border intersection. The Laurentide – Cordilleran saddle is fully developed at 25 ka in the NADI-1_max reconstruction, leading to ~650 m of subsidence relative to present day until ~15 ka.

When we compare to the ICE-7G, NAICE, and LW-6 reconstructions, we find differences reach up to ~750 m (Fig. 9). Larger differences in paleotopography predictions between previous reconstructions and our new ICE-NADI-1 reconstructions reflect the fact that there are greater discrepancies in ice sheet volume, in addition to the timing and magnitude of retreat, among the previous reconstructions compared to our new ICE-NADI-1 ice sheet reconstructions. Notable discrepancies in paleotopography predictions among GIA simulations with our new North American ice sheet reconstructions are also evident in southwest and southcentral Alaska (Sukoi Bay) and the Great Lakes region (central Michigan) (Fig. 9; Text S3).

https://doi.org/10.5194/egusphere-2026-4374
Preprint. Discussion started: 29 July 2026

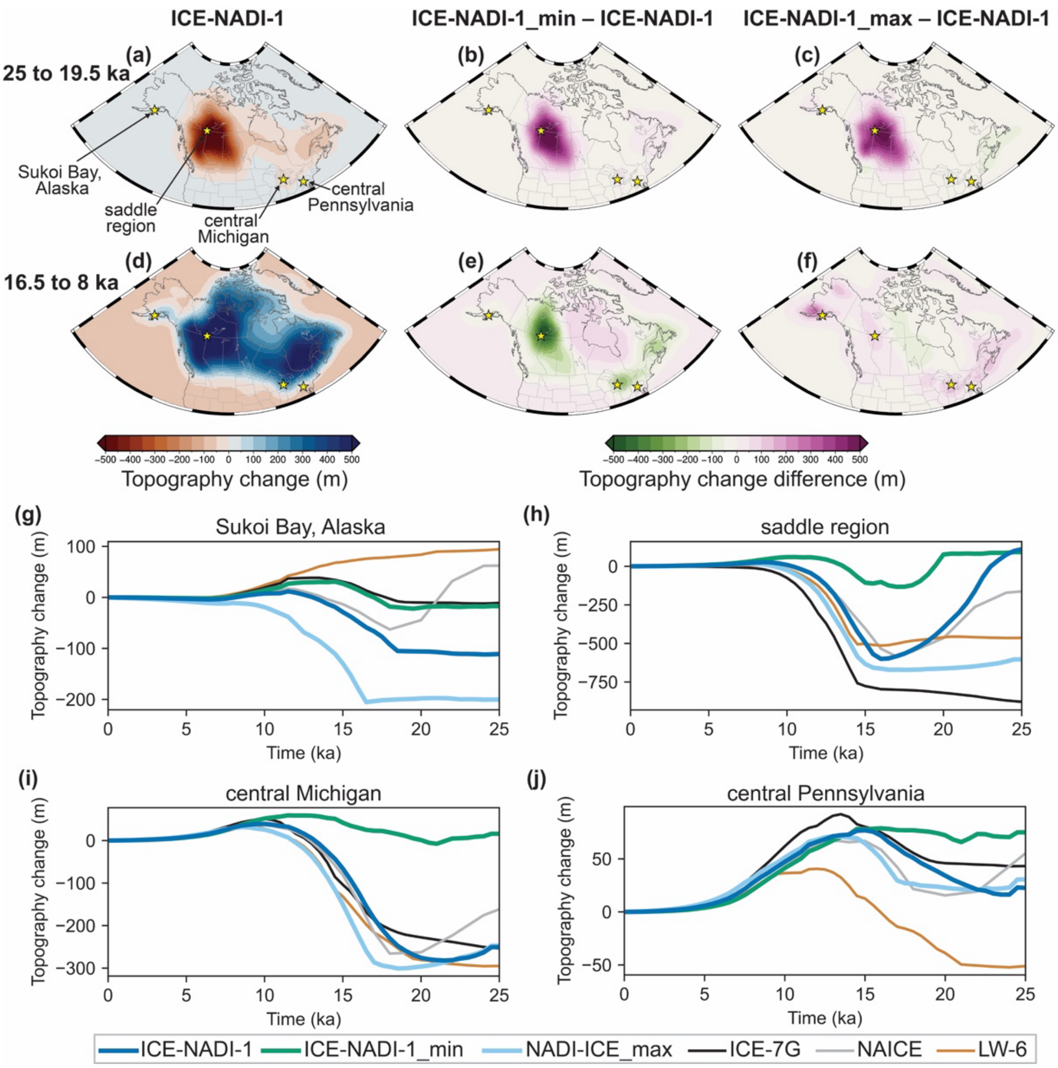

Figure 9. Paleotopography predictions from glacial isostatic adjustment simulations with the ICE-NADI-1 reconstructions. (a) Paleotopography change from 25 to 19.5 ka (19.5 ka minus 25 ka) predicted in a GIA simulation with ICE-NADI-1. (b-c) Difference in paleotopography predictions from 25 to 19.5 ka between GIA simulations adopting (b) ICE-NADI-1_min versus ICE-NADI-1 and (c) ICE-NADI-1_max versus ICE-NADI-1. (d-f) Same as (a-c) but for 16.5 to 8 ka. (g-j) Topography change time series from 25 ka to 0 ka locations of interest, including (g) in the Alaskan sector of the Cordilleran Ice Sheet (Sukoi Bay, Alaska), (h) in the Laurentide-Cordilleran saddle region (saddle region), (i) the southern extent of the Laurentide Ice Sheet (central Michigan), and (j) just beyond the southern extent of the Laurentide Ice Sheet (central Pennsylvania). The locations are marked by stars in (a-f) and move progressively eastward from (g) to (j). All GIA simulations use the Earth_1 model.

3.4.3 Present-day vertical land motion from GIA

GIA is a major contributor to present-day vertical land motion across North America and produces observable signals in GNSS and GRACE data (e.g., Sella et al., 2007; van der Wal et al., 2008; Caron et al., 2018; Hightower et al., 2026). Efforts have illustrated how different representations of solid Earth structure impact predictions of present-day vertical land motion and the contemporary gravitational signal of GIA (e.g., Caron et al., 2018; Williams et al., 2024; Brierley-Green & James, 2025;

https://doi.org/10.5194/egusphere-2026-4374
Preprint. Discussion started: 29 July 2026

Hightower et al., 2026). However, these studies have all adopted ice sheet reconstructions developed using the Dyke (2004) North American ice margins (e.g., ICE-7G, ICE-6G-D, LW-6) in their GIA modeling approaches. In Figure 10, we plot present-day vertical crustal motion rates predicted in simulations with the ICE-NADI-1, ICE-7G, and LW-6 reconstructions. We find that the spatial pattern and magnitude of vertical crustal motion rate predictions due to GIA strongly depend on the adopted ice sheet reconstruction, with up to 9 mm/year difference in North America between simulations adopting ICE-NADI-1, ICE-7G, and LW-6 with identical Earth models (Earth_1).

Uncertainty associated with the NADI-1 margins also translates to uncertainty in present-day vertical crustal motion predictions. We find up to 21 mm/year difference in vertical crustal motions rates between the ICE-NADI-1 and ICE-NADI-1_max reconstruction. Discrepancies in vertical crustal motions between ICE-NADI-1 and ICE-NADI-1_min are smaller, only reaching up to 3.7 mm/year. Recently, Hightower et al. (2026) investigated the sensitivity of vertical crustal motion predictions to different 1-D and 3-D Earth structure realizations and demonstrated that varying Earth structure can lead to differences in vertical crustal motion predictions reaching up to ~5 mm/year in North America. Therefore, the sensitivity of vertical crustal motions to the choice of ice sheet reconstruction is comparable to, and often greater than, the sensitivity to different plausible Earth structure realizations. Thus, future studies that aim to improve predictions of vertical land motion and the gravitational signal associated with ongoing GIA should consider a wider range of plausible ice sheet reconstructions.

https://doi.org/10.5194/egusphere-2026-4374
Preprint. Discussion started: 29 July 2026

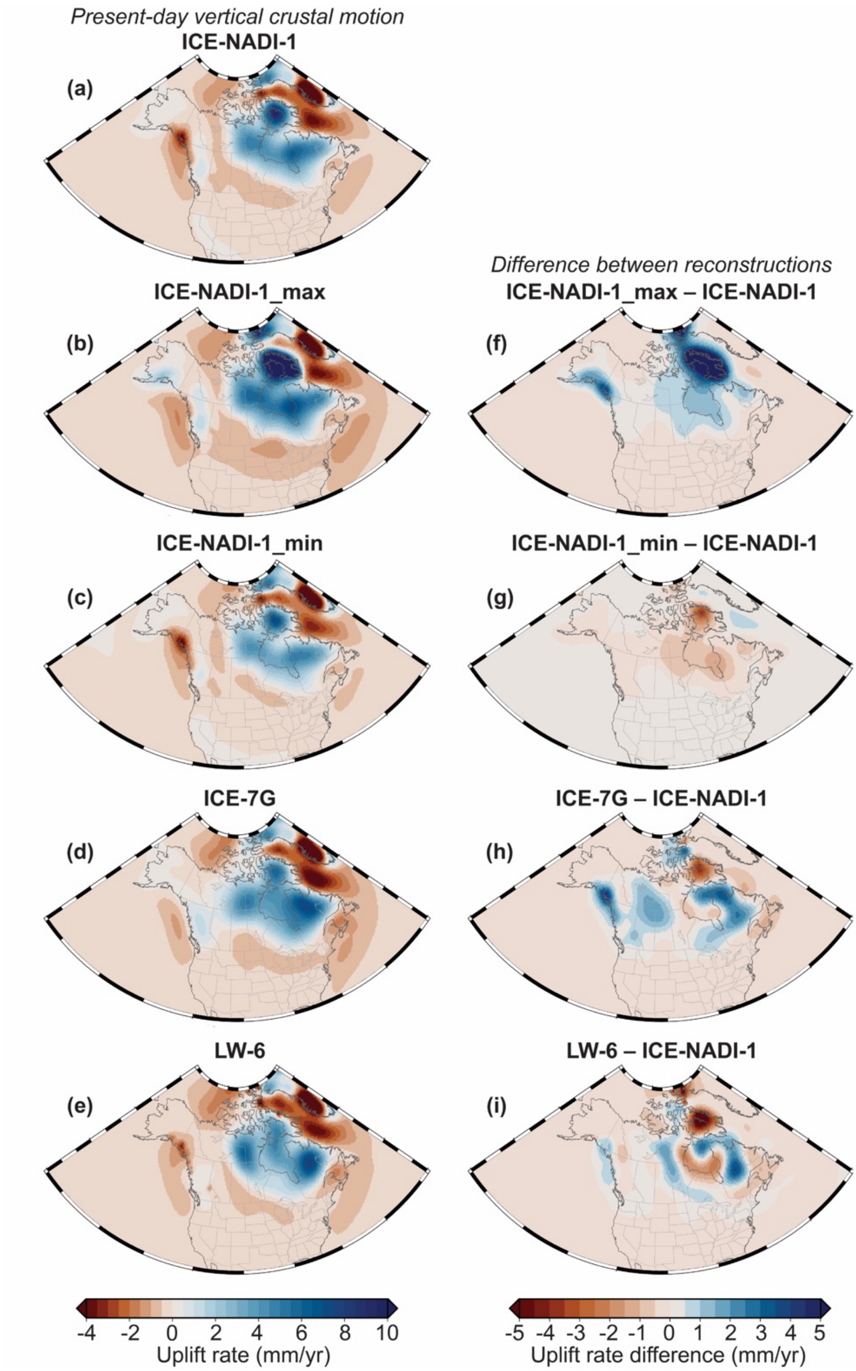

500 **Figure 10. Present-day vertical crustal motion rates due to glacial isostatic adjustment in North America.** (a-e) GIA vertical crustal motion rates from simulations adopting the (a) ICE-NADI-1, (b) ICE-NADI-1_max, (c), ICE-NADI-1_min, (d) ICE-7G, and (e) LW-6 reconstructions. Vertical crustal motion rates computed using predicted radial displacement from 0.5 to 0 ka and dividing by 500 years. (f-i) Difference in present-day vertical crustal motion rates between (f) ICE-NADI-1_max and ICE-NADI-1, (g) ICE-NADI-1_min and ICE-NADI-1, (h) ICE-7G and ICE-NADI-1, and (i) LW-6 and ICE-NADI-1.

https://doi.org/10.5194/egusphere-2026-4374
Preprint. Discussion started: 29 July 2026

4 Conclusions

We developed three new deglacial North American Ice Sheet Complex reconstructions (ICE-NADI-1, ICE-NADI-1_max, and ICE-NADI-1_min) using a simple, steady-state ice sheet model with the empirically derived North American Deglaciation Isochrones (NADI-1; Dalton et al., 2023) optimal, minimum, and maximum margins. Our reconstructions illustrate how 2-D ice margins influence the history of 3-D ice volume evolution, granting new insight into North American Ice Sheet Complex dynamics and global sea-level contributions over the past 25 ka.

We find that ICE-NADI-1 contributes 6.3 m SLE from North America to MWP-1a, in contrast to contributions of 16 m SLE and 14 m SLE in ICE-7G and LW-6, respectively, with a peak ice loss rate (13 mm SLE/year) less than half the rate of ice loss in ICE-7G and LW-6. ICE-NADI-1 contains a peak North American sea-level equivalent (SLE) ice volume of 64 m at the Last Glacial Maximum, 25% smaller than the North American ice volume contained within ICE-7G (Roy & Peltier, 2017). Furthermore, North American ice saddle merging, which is not captured in ICE-7G or LW-6, contributes 13 m SLE to global sea-level fall leading into the LGM. Our empirically-informed ice thickness reconstructions reduce estimates for North American ice volume and its sea-level contributions, consistent with recent studies that support a short-lived LGM lowstand (Yokoyama et al., 2018; Vacchi et al., 2025) and a smaller North American ice melt contribution to MWP-1a (Coonin et al., 2025; Brendryen et al., 2020; Lin et al., 2021; Stoker et al., 2022; Norris et al., 2022).

Our ICE-NADI-1 reconstructions fit North American RSL observations as well or better than previous North American Ice Sheet Complex reconstructions (ICE-7G, LW-6, NAICE). Unlike previous reconstructions, uncertainty bounds on NADI-1 ice margins permit a quantitative assessment of the sensitivity of glacial isostatic adjustment predictions to ice geometry, which we find comparable in magnitude to uncertainty related to Earth structure. We find that our ICE-NADI-1 reconstruction impacts present-day vertical land motion due to GIA, differing from previous predictions by up to 9 mm/year. Our new publicly available ICE-NADI-1 ice sheet thickness reconstructions will be useful for future GIA modeling studies and paleoclimate modeling studies for North America.

Code and data availability

The ICE-NADI-1, ICE-NADI-1_min, and ICE-NADI-1_max ice sheet reconstructions and paleotopography predictions are publicly available at https://doi.org/10.5281/zenodo.21142280.

https://doi.org/10.5194/egusphere-2026-4374
Preprint. Discussion started: 29 July 2026

Author contributions

Conceptualization: EML, SK, TP. Formal analysis: EML, SK, TP. Methodology: EML, SK, TP. Project administration: EML and TP. Supervision: TP. Investigation: all. Visualization: EML, TP, SK. Funding acquisition: TP. Writing (original draft): EML and TP. Writing (reviewing and editing): all.

Competing interests

None of the authors have any competing interests.

Acknowledgements

TP, EML, and SK acknowledge funding from NSF OCE – 2054757.

References

Afonso, J. C., Salajegheh, F., Szwillus, W., Ebbing, J., and Gaina, C.: A global reference model of the lithosphere and upper mantle from joint inversion and analysis of multiple data sets, Geophys J Int, 217, 1602–1628, https://doi.org/10.1093/gji/ggz094, 2019.

Austermann, J., Chen, C. Y., Lau, H. C. P., Maloof, A. C., and Latychev, K.: Constraints on mantle viscosity and Laurentide ice sheet evolution from pluvial paleolake shorelines in the western United States, Earth and Planetary Science Letters, 532, 116006, https://doi.org/10.1016/j.epsl.2019.116006, 2020.

Austermann, J., Mitrovica, J. X., Latychev, K., and Milne, G. A.: Barbados-based estimate of ice volume at Last Glacial Maximum affected by subducted plate. Nature Geoscience, 6(7), 553–557. https://doi.org/10.1038/ngeo1859, 2013.

Austermann, J., Hoggard, M. J., Latychev, K., Richards, F. D., and Mitrovica, J. X.: The effect of lateral variations in Earth structure on Last Interglacial sea level, Geophys J Int, 227, 1938–1960, https://doi.org/10.1093/gji/ggab289, 2021.

Austermann, J., Wickert, A. D., Pico, T., Kingslake, J., Callaghan, K. L., and Creel, R. C.: Glacial Isostatic Adjustment Shapes Proglacial Lakes Over Glacial Cycles, Geophysical Research Letters, 49, e2022GL101191, https://doi.org/10.1029/2022GL101191, 2022.

Bradley, S. L., Ely, J. C., Clark, C. D., Edwards, R. J., and Shennan, I.: Reconstruction of the palaeo-sea level of Britain and Ireland arising from empirical constraints of ice extent: implications for regional sea level forecasts and North American ice sheet volume, Journal of Quaternary Science, 38, 791–805, https://doi.org/10.1002/jqs.3523, 2023.

Brendryen, J., Haflidason, H., Yokoyama, Y., Haaga, K. A., and Hannisdal, B.: Eurasian Ice Sheet collapse was a major source of Meltwater Pulse 1A 14,600 years ago. Nature Geoscience, 13, 5, 363–368. https://doi.org/10.1038/s41561-020-0567-4, 2020.

Brierley-Green, C. and James, T. S.: Effect of lithospheric thickness and radial mantle viscosity profile on glacial isostatic adjustment crustal motions in North America. Canadian Journal of Earth Sciences, 62(4), 875–891. https://doi.org/10.1139/cjes-2024-0118, 2025.

Caron, L., Ivins, E. R., Larour, E., Adhikari, S., Nilsson, J., and Blewitt, G.: GIA Model Statistics for GRACE Hydrology, Cryosphere, and Ocean Science, Geophysical Research Letters, 45, 2203–2212, https://doi.org/10.1002/2017GL076644, 2018.

Clark, P. U., Dyke, A. S., Shakun, J. D., Carlson, A. E., Clark, J., Wohlfarth, B., Mitrovica, J. X., Hostetler, S. W., and McCabe, A. M.: The Last Glacial Maximum. Science, 325, 5941, 710–714. https://doi.org/10.1126/science.1172873, 2009.

Dalton, A. S., Dulfer, H. E., Margold, M., Heyman, J., Clague, J. J., Froese, D. G., Gauthier, M. S., Hughes, A. L. C., Jennings, C. E., Norris, S. L., and Stoker, B. J.: Deglaciation of the north American ice sheet complex in calendar years based on a comprehensive database of chronological data: NADI-1, Quaternary Science Reviews, 321, 108345, https://doi.org/10.1016/j.quascirev.2023.108345, 2023.

Deschamps, P., Durand, N., Bard, E., Hamelin, B., Camoin, G., Thomas, A. L., Henderson, G. M., Okuno, J., and Yokoyama, Y.: Ice-sheet collapse and sea-level rise at the Bølling warming 14,600 years ago, Nature, 483, 559–564, https://doi.org/10.1038/nature10902, 2012.

Dyke, A. S.: An outline of North American deglaciation with emphasis on central and northern Canada, in: Developments in Quaternary Sciences, vol. 2, Elsevier, 373–424, https://doi.org/10.1016/S1571-0866(04)80209-4, 2004.

Dyke, A. S., Moore, A. and Robertson, L.: Deglaciation of North America: Thirty-two digital maps at 1:7,000,000 scale with accompanying digital chronological database and one poster (two sheets) with full map series, Geol. Surv. Can. Open File, 1574, https://doi.org/10.4095/214399, 2003.

Dziewonski, A. M. and Anderson, D. L.: Preliminary reference Earth model, Physics of the Earth and Planetary Interiors, 25, 297–356, https://doi.org/10.1016/0031-9201(81)90046-7, 1981.

Engelhart, S. E. and Horton, B. P.: Holocene sea level database for the Atlantic coast of the United States, Quaternary Science Reviews, 54, 12–25, https://doi.org/10.1016/j.quascirev.2011.09.013, 2012.

Engelhart, S. E., Vacchi, M., Horton, B. P., Nelson, A. R., and Kopp, R. E.: A sea-level database for the Pacific coast of central North America, Quaternary Science Reviews, 113, 78–92, https://doi.org/10.1016/j.quascirev.2014.12.001, 2015.

Fisher, D., Reeh, N., Langley, K.: Objective reconstructions of the Late Wisconsinan Laurentide Ice Sheet and the significance of deformable beds. Géogr. Phys. Quat, 39, 229-238, 1985.

Gauthier, M. S., Kelley, S. E., and Hodder, T. J.: Lake Agassiz drainage bracketed Holocene Hudson Bay Ice Saddle collapse, Earth and Planetary Science Letters, 544, 116372, https://doi.org/10.1016/j.epsl.2020.116372, 2020.

Gowan, E. J., Tregoning, P., Purcell, A., Lea, J., Fransner, O. J., Noormets, R., and Dowdeswell, J. A.: ICESHEET 1.0: a program to produce paleo-ice sheet reconstructions with minimal assumptions, Geoscientific Model Development, 9, 1673–1682, https://doi.org/10.5194/gmd-9-1673-2016, 2016a.

Gowan, E. J., Tregoning, P., Purcell, A., Montillet, J.-P., and McClusky, S.: A model of the western Laurentide Ice Sheet, using observations of glacial isostatic adjustment, Quaternary Science Reviews, 139, 1–16, https://doi.org/10.1016/j.quascirev.2016.03.003, 2016b.

Gregoire, L. J., Otto-Bliesner, B., Valdes, P. J., and Ivanovic, R.: Abrupt Bølling warming and ice saddle collapse contributions to the Meltwater Pulse 1a rapid sea level rise, Geophysical Research Letters, 43, 9130–9137, https://doi.org/10.1002/2016GL070356, 2016.

Hanebuth, T., Stattegger, K., and Grootes, P. M.: Rapid flooding of the sunda shelf: A late-glacial sea-level record, Science, 288, 1033–1035, https://doi.org/10.1126/science.288.5468.1033, 2000.

Hanebuth, T. J. J., Stattegger, K., & Bojanowski, A.: Termination of the Last Glacial Maximum sea-level lowstand: The Sunda-Shelf data revisited. Global and Planetary Change, Quaternary Sea-Level Changes Records and Processes, 66, 1, 76–84. https://doi.org/10.1016/j.gloplacha.2008.03.011, 2009.

Hightower, E., Caron, L., Landerer, F., Watkins, M., Ivins, E., and Larour, E.: Impact of Heterogeneous Mantle Viscosity on the Glacial Isostatic Adjustment Correction for GRACE(-FO): Implications for Surface Mass Trends. https://doi.org/10.22541/essoar.15004543/v1, 2026.

Hijma, M. P. and Cohen, K. M.: Holocene sea-level database for the Rhine-Meuse Delta, The Netherlands: Implications for the pre-8.2 ka sea-level jump, Quaternary Science Reviews, 214, 68–86, https://doi.org/10.1016/j.quascirev.2019.05.001, 2019.

Hijma, M. P., Bradley, S. L., Cohen, K. M., van der Wal, W., Barlow, N. L. M., Blank, B., Frechen, M., Hennekam, R., van Heteren, S., Kiden, P., Mavritsakis, A., Meijninger, B. M. L., Reichart, G.-J., Reinhardt, L., Rijsdijk, K. F., Vink, A., and Busschers, F. S.: Global sea-level rise in the early Holocene revealed from North Sea peats, Nature, 639, 652–657, https://doi.org/10.1038/s41586-025-08769-7, 2025.

Ishiwa, T., Yokoyama, Y., Miyairi, Y., Obrochta, S., Sasaki, T., Kitamura, A., Suzuki, A., Ikehara, M., Ikehara, K., Kimoto, K., Bourget, J., and Matsuzaki, H.: Reappraisal of sea-level lowstand during the Last Glacial Maximum observed in the Bonaparte Gulf sediments, northwestern Australia, Quaternary International, 397, 373–379, https://doi.org/10.1016/j.quaint.2015.03.032, 2016.

Johnston, P.: The effect of spatially non-uniform water loads on prediction of sea-level change, Geophys J Int, 114, 615–634, https://doi.org/10.1111/j.1365-246X.1993.tb06992.x, 1993.

Kendall, R. A., Mitrovica, J. X., and Milne, G. A.: On post-glacial sea level – II. Numerical formulation and comparative results on spherically symmetric models, Geophys J Int, 161, 679–706, https://doi.org/10.1111/j.1365-246X.2005.02553.x, 2005.

Kodama, S. T., Pico, T., Finnegan, N. J., Lapôtre, M. G. A., and Willenbring, J. K.: Glacial Isostatic Adjustment Modulates Lateral Migration Rate and Morphology of the Red River (North Dakota, USA and Manitoba, Canada), Geophysical Research Letters, 50, e2023GL103995, https://doi.org/10.1029/2023GL103995, 2023.

Lambeck, K., Purcell, A., Johnston, P., Nakada, M., and Yokoyama, Y.: Water-load definition in the glacio-hydro-isostatic sea-level equation, Quaternary Science Reviews, 22, 309–318, https://doi.org/10.1016/S0277-3791(02)00142-7, 2003.

Lambeck, K., Rouby, H., Purcell, A., Sun, Y., and Sambridge, M.: Sea level and global ice volumes from the Last Glacial Maximum to the Holocene, Proceedings of the National Academy of Sciences, 111, 15296–15303, https://doi.org/10.1073/pnas.1411762111, 2014.

Lambeck, K., Purcell, A., and Zhao, S.: The North American Late Wisconsin ice sheet and mantle viscosity from glacial rebound analyses, Quaternary Science Reviews, 158, 172–210, https://doi.org/10.1016/j.quascirev.2016.11.033, 2017.

Li, T., Wu, P., Wang, H., Steffen, H., Khan, N. S., Engelhart, S. E., Vacchi, M., Shaw, T. A., Peltier, W. R., and Horton, B. P.: Uncertainties of Glacial Isostatic Adjustment Model Predictions in North America Associated With 3D Structure, Geophysical Research Letters, 47, e2020GL087944, https://doi.org/10.1029/2020GL087944, 2020.

Lin, Y., Hibbert, F. D., Whitehouse, P. L., Woodroffe, S. A., Purcell, A., Shennan, I., and Bradley, S. L.: A reconciled solution of Meltwater Pulse 1A sources using sea-level fingerprinting, Nat Commun, 12, 2015, https://doi.org/10.1038/s41467-021-21990-y, 2021.

Love, R., Milne, G. A., Tarasov, L., Engelhart, S. E., Hijma, M. P., Latychev, K., Horton, B. P., and Törnqvist, T. E.: The contribution of glacial isostatic adjustment to projections of sea-level change along the Atlantic and Gulf coasts of North America, Earth's Future, 4, 440–464, https://doi.org/10.1002/2016EF000363, 2016.

Marsman, C. P., van der Wal, W., Riva, R. E. M., and Freymueller, J. T.: The Impact of a 3-D Earth Structure on Glacial Isostatic Adjustment in Southeast Alaska Following the Little Ice Age, Journal of Geophysical Research: Solid Earth, 126, e2021JB022312, https://doi.org/10.1029/2021JB022312, 2021.

Lucas, E. M., Kodama, S., Pico, T., Stoker, B. S., Lesnek, A., and Dalton, A. S.: Data from: ICE-NADI-1: A new deglacial ice sheet thickness history (25-1 ka) for North America using empirically-constrained ice margins with implications for global sea-level contributions, relative sea level, and vertical land motion [Dataset]. Zenodo. https://doi.org/10.5281/zenodo.21464139.

Melini, D. and Spada, G.: Some remarks on Glacial Isostatic Adjustment modelling uncertainties, Geophys J Int, 218, 401–413, https://doi.org/10.1093/gji/ggz158, 2019.

Milne, G. A., Mitrovica, J. X., and Davis, J. L.: Near-field hydro-isostasy: the implementation of a revised sea-level equation, Geophys J Int, 139, 464–482, https://doi.org/10.1046/j.1365-246x.1999.00971.x, 1999.

Mitrovica, J. X. and Forte, A. M.: A new inference of mantle viscosity based upon joint inversion of convection and glacial isostatic adjustment data, Earth and Planetary Science Letters, 225, 177–189, https://doi.org/10.1016/j.epsl.2004.06.005, 2004.

Mukherjee, U., Vetter, L., Milne, G. A., Tarasov, L., Steponaitis, E., Cahill, N., Lecavalier, B. S., Rosenheim, B. E., and Törnqvist, T. E.: Sea-level rise at the end of the last deglaciation dominated by North American ice sheets, Nat. Geosci., 18, 1167–1173, https://doi.org/10.1038/s41561-025-01806-0, 2025.

Norris, S. L., Tarasov, L., Monteath, A. J., Gosse, J. C., Hidy, A. J., Margold, M., and Froese, D. G.: Rapid retreat of the southwestern Laurentide Ice Sheet during the Bølling-Allerød interval. Geology, 50(4), 417–421. https://doi.org/10.1130/G49493.1, 2022.

Parang, S., Milne, G. A., Tarasov, L., Love, R., Yousefi, M., and Vacchi, M.: Constraining models of glacial isostatic adjustment in eastern North America, Quaternary Science Reviews, 334, 108708, https://doi.org/10.1016/j.quascirev.2024.108708, 2024.

Peltier, W. R.: Global Glacial Isostasy and the Surface of the Ice-Age Earth: The ICE-5G (VM2) Model and GRACE, Annual Review of Earth and Planetary Sciences, 32, 111–149, https://doi.org/10.1146/annurev.earth.32.082503.144359, 2004.

Peltier, W. R. and Fairbanks, R. G.: Global glacial ice volume and Last Glacial Maximum duration from an extended Barbados sea level record, Quaternary Science Reviews, 25, 3322–3337, https://doi.org/10.1016/j.quascirev.2006.04.010, 2006.

Peltier, W. R., Argus, D. F., and Drummond, R.: Space geodesy constrains ice age terminal deglaciation: The global ICE-6G_C (VM5a) model, Journal of Geophysical Research: Solid Earth, 120, 450–487, https://doi.org/10.1002/2014JB011176, 2015.

Pollard, O. G., Barlow, N. L. M., Gregoire, L. J., Gomez, N., Cartelle, V., Ely, J. C., and Astfalck, L. C.: Quantifying the uncertainty in the Eurasian ice-sheet geometry at the Penultimate Glacial Maximum (Marine Isotope Stage 6), The Cryosphere, 17, 4751–4777, https://doi.org/10.5194/tc-17-4751-2023, 2023.

Reyes, A. V., Carlson, A. E., Clark, J., Guillaume, L., Milne, G. A., Tarasov, L., Carlson, E. C. B., He, F., Caffee, M. W., Wilcken, K. M., and Rood, D. H.: Timing of Cordilleran-Laurentide ice-sheet separation: Implications for sea-level rise, Quaternary Science Reviews, 328, 108554, https://doi.org/10.1016/j.quascirev.2024.108554, 2024.

Roy, K. and Peltier, W. R.: Glacial isostatic adjustment, relative sea level history and mantle viscosity: reconciling relative sea level model predictions for the U.S. East coast with geological constraints, Geophys J Int, 201, 1156–1181, https://doi.org/10.1093/gji/ggv066, 2015.

Roy, K. and Peltier, W. R.: Space-geodetic and water level gauge constraints on continental uplift and tilting over North America: regional convergence of the ICE-6G_C (VM5a/VM6) models, Geophys J Int, 210, 1115–1142, https://doi.org/10.1093/gji/ggx156, 2017.

Roy, K. and Peltier, W. R.: Relative sea level in the Western Mediterranean basin: A regional test of the ICE-6G_C_NA (VM7) model and a constraint on late Holocene Antarctic deglaciation, Quaternary Science Reviews, 183, 76–87, https://doi.org/10.1016/j.quascirev.2017.12.021, 2018.

Rush, G., Garrett, E., Bateman, M. D., Bigg, G. R., Hibbert, F. D., Smith, D. E., and Gehrels, W. R.: The magnitude and source of meltwater forcing of the 8.2 ka climate event constrained by relative sea-level data from eastern Scotland, Quaternary Science Advances, 12, 100119, https://doi.org/10.1016/j.qsa.2023.100119, 2023.

Sanborn, L. H., Pico, T., Donnelly, J. P., and Perron, J. T.: Glacial isostatic adjustment shifted early Holocene river hydrology in Maine, USA, Geology, 53, 446–450, https://doi.org/10.1130/G52822.1, 2025.

Sella, G. F., Stein, S., Dixon, T. H., Craymer, M., James, T. S., Mazzotti, S., and Dokka, R. K.: Observation of glacial isostatic adjustment in "stable" North America with GPS, Geophysical Research Letters, 34, https://doi.org/10.1029/2006GL027081, 2007.

Simon, K. M., James, T. S., Henton, J. A., and Dyke, A. S.: A glacial isostatic adjustment model for the central and northern Laurentide Ice Sheet based on relative sea level and GPS measurements, Geophys J Int, 205, 1618–1636, https://doi.org/10.1093/gji/ggw103, 2016.

Simon, K. M., Riva, R. E. M., Kleinherenbrink, M., and Tangdamrongsub, N.: A data-driven model for constraint of present-day glacial isostatic adjustment in North America, Earth and Planetary Science Letters, 474, 322–333, https://doi.org/10.1016/j.epsl.2017.06.046, 2017.

Stoker, B. J., Margold, M., Gosse, J. C., Hidy, A. J., Monteath, A. J., Young, J. M., Gandy, N., Gregoire, L. J., Norris, S. L., and Froese, D.: The collapse of the Cordilleran–Laurentide ice saddle and early opening of the Mackenzie Valley, Northwest Territories, Canada, constrained by 10Be exposure dating. The Cryosphere, 16, 12, 4865–4886. https://doi.org/10.5194/tc-16-4865-2022, 2022.

Vacchi, M., Engelhart, S. E., Nikitina, D., Ashe, E. L., Peltier, W. R., Roy, K., Kopp, R. E., and Horton, B. P.: Postglacial relative sea-level histories along the eastern Canadian coastline, Quaternary Science Reviews, 201, 124–146, https://doi.org/10.1016/j.quascirev.2018.09.043, 2018.

van der Wal, W., Wu, P., Sideris, M. G., and Shum, C. K.: Use of GRACE determined secular gravity rates for glacial isostatic adjustment studies in North-America, Journal of Geodynamics, 46, 144–154, https://doi.org/10.1016/j.jog.2008.03.007, 2008.

Williams, K., Stamps, D. S., Melini, D., and Spada, G.: Vertical Displacements and Sea-Level Changes in Eastern North America Driven by Glacial Isostatic Adjustment: An Ensemble Modeling Approach, Journal of Geophysical Research: Solid Earth, 129, e2023JB028250, https://doi.org/10.1029/2023JB028250, 2024.

Yokoyama, Y., Lambeck, K., De Deckker P, null, Johnston, P., and Fifield, L. K.: Timing of the Last Glacial Maximum from observed sea-level minima, Nature, 406, 713–716, https://doi.org/10.1038/35021035, 2000.

Yokoyama, Y., Esat, T. M., Thompson, W. G., Thomas, A. L., Webster, J. M., Miyairi, Y., Sawada, C., Aze, T., Matsuzaki, H., Okuno, J., Fallon, S., Braga, J.-C., Humblet, M., Iryu, Y., Potts, D. C., Fujita, K., Suzuki, A., and Kan, H.: Rapid glaciation and a two-step sea level plunge into the Last Glacial Maximum, Nature, 559, 603–607, https://doi.org/10.1038/s41586-018-0335-4, 2018.

You, D., Stein, R., Fahl, K., Williams, M. C., Schmidt, D. N., McCave, I. N., Barker, S., Schefuß, E., Niu, L., Kuhn, G., and Niessen, F.: Last deglacial abrupt climate changes caused by meltwater pulses in the Labrador Sea, Commun Earth Environ, 4, 81, https://doi.org/10.1038/s43247-023-00743-3, 2023.

Yousefi, M., Milne, G. A., Love, R., and Tarasov, L.: Glacial isostatic adjustment along the Pacific coast of central North America, Quaternary Science Reviews, 193, 288–311, https://doi.org/10.1016/j.quascirev.2018.06.017, 2018.